



# Laser powder bed fusion to fabricate high-entropy alloy FeCoCrNiMo<sub>0.5</sub> with excellent high-temperature strength and ductility



Danyang Lin<sup>a,b</sup>, Qi Chen<sup>a,b</sup>, Xin Xi<sup>a,b</sup>, Rui Ma<sup>c</sup>, Zhifeng Shi<sup>c</sup>, Xiaoguo Song<sup>a,b,\*</sup>, Hongbo Xia<sup>a,d,\*\*</sup>, Hong Bian<sup>a,b</sup>, Caiwang Tan<sup>a,b</sup>, Yongxin Lu<sup>e</sup>, Runsheng Li<sup>f</sup>

<sup>a</sup> National Key Laboratory of Precision Welding & Joining of Materials and Structures, Harbin Institute of Technology, Harbin, 150001, China

<sup>b</sup> Shandong Provincial Key Laboratory of Special Welding Technology, Harbin Institute of Technology Weihai, Weihai, 264209, China

<sup>c</sup> Beijing Power Machinery Institute, Beijing, 100000, China

<sup>d</sup> Zhengzhou Research Institute, Harbin Institute of Technology, Zhengzhou, 450018, China

<sup>e</sup> School of Material Science and Engineering, Xi'an Shiyou University, Xi'an, 710065, China

<sup>f</sup> College of Mechanical and Electronic Engineering, China University of Petroleum (East China), Qingdao, 266580, China

## ARTICLE INFO

### Keywords:

Laser powder bed fusion  
High-entropy alloy  
High-temperature mechanical properties  
Strengthening mechanism

## ABSTRACT

FeCoCrNi, a high-entropy alloy fabricated by laser powder bed fusion, has excellent room-temperature mechanical properties but poor high-temperature mechanical performance. To expand the application of FeCoCrNi, in this study, we added Mo to form  $\sigma$  precipitates, which improved the high-temperature mechanical properties of the alloy via Orowan strengthening. We also elucidated the main deformation mechanism of FeCoCrNiMo<sub>0.5</sub>, involving the transformation of the deformational mode from dislocation-based motion to twinning deformation.

## 1. Introduction

Metallic materials exhibit increased plasticity and decreased strength at elevated temperatures because dislocation motion and grain boundary (GB) slip are facilitated by the augmented atomic diffusion and weakened atomic bonding of metal species at higher temperatures [1–4]. High-entropy alloys (HEAs), originally defined as consisting of five elements with equal or nearly equal atomic proportions [5–7], have been extensively investigated as high-performance materials with high strength, high hardness, and high-temperature oxidation resistance [8–13]. With the improved understanding of HEAs, it has been noted that the above definition cannot accurately account for all the characteristics of HEAs, and the precise definition of HEAs is being reconsidered. Among the different HEAs, FeCoCrNi HEAs have been the most widely studied candidates. Laser powder bed fusion (LPBF) with the characteristics of direct forming is an advanced manufacturing technology for fabricating structural materials with high precision in a short time [14–16]. The LPBF method for preparing FeCoCrNi HEA components overcomes the difficulty associated with the deformation of high-strength alloys [17]. In addition, LPBF-FeCoCrNi HEAs exhibit better room-temperature mechanical performance than the HEAs

prepared using conventional methods [18–21]. However, they still show a softening phenomenon at high operational temperature [21]. Therefore, it is imperative to improve the high-temperature strengths of LPBF-FeCoCrNi HEAs.

The performance of FeCoCrNi HEAs is typically improved by compositional modification with the addition of other elements, such as Al [22,23], Si [24], Mo [25–29], Mn [30], Nb [31,32], and W [33]. Although the addition of certain elements, such as Al, Si, Mn, and Nb, significantly changes the room-temperature strength of FeCoCrNi HEAs, high-temperature softening is also clearly noticed. In certain cases, a significant reduction in their high-temperature plasticity is observed. The addition of Mo has unique effects on FeCoCrNi HEAs, because it induces the formation of a hard intermetallic  $\sigma$  phase [25–28], which promotes the solid-solution and precipitation strengthening phenomena, thereby significantly increasing both the yield and tensile strengths of the HEA. In addition, compared with other alloys, FeCoCrNiMo HEAs exhibit improved elongation and ductility. Peng et al. [26] successfully synthesized completely dense FeCoCrNiMo HEAs using two processes, viz., spark plasma sintering and vacuum hot-press sintering, and reported that FeCoCrNiMo HEAs have excellent hardness and wear resistance but poor strength and plasticity owing to the precipitation of hard

\* Corresponding author. State Key Laboratory of Advanced Welding and Joining, Harbin Institute of Technology, Harbin, 150001, China.

\*\* Corresponding author. State Key Laboratory of Advanced Welding and Joining, Harbin Institute of Technology, Harbin, 150001, China.

E-mail addresses: [xgsong@hitwh.edu.cn](mailto:xgsong@hitwh.edu.cn) (X. Song), [xiahongbo@hit.edu.cn](mailto:xiahongbo@hit.edu.cn) (H. Xia).

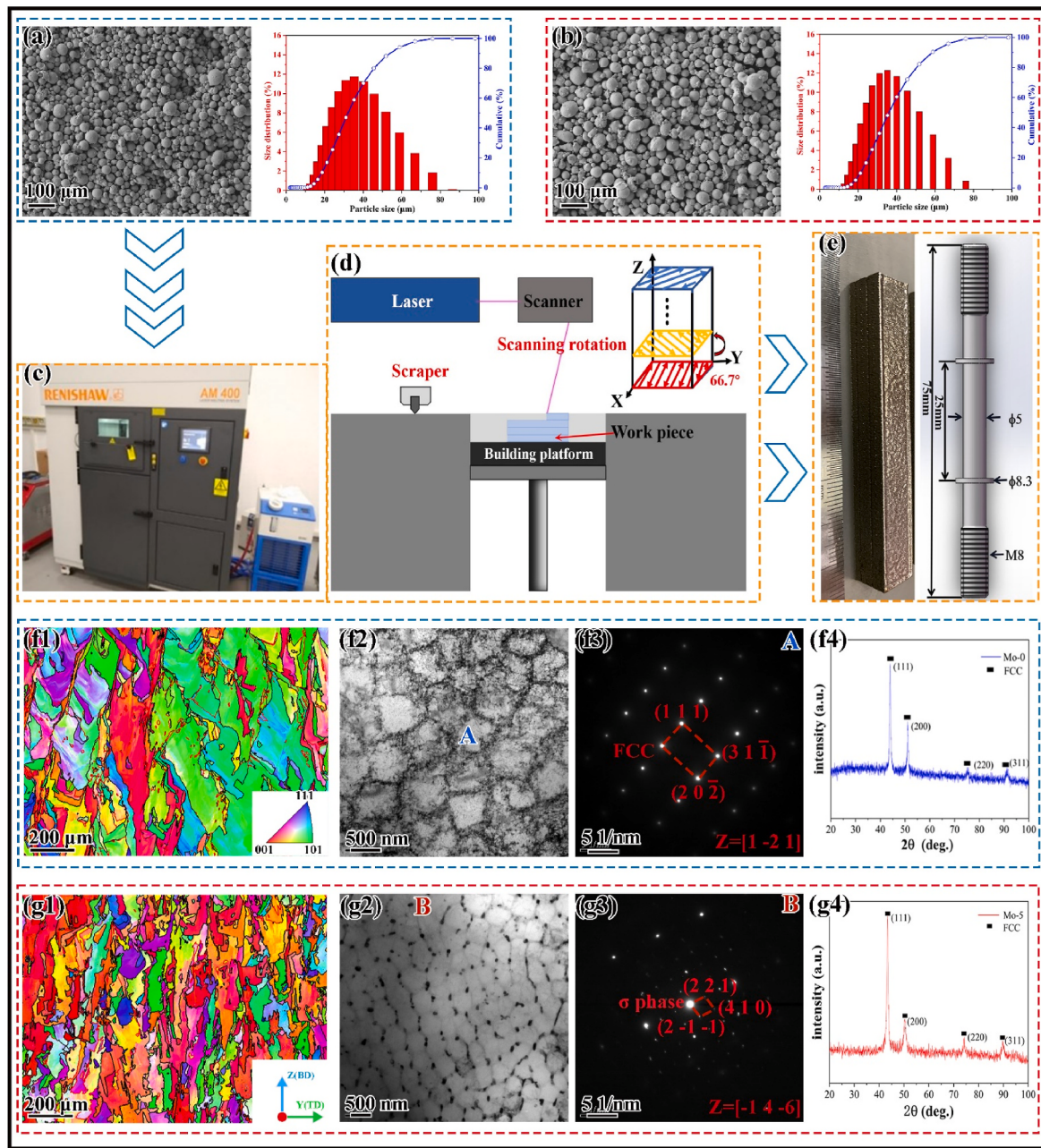


**Fig. 1.** Scanning electron microscopy (SEM) images and particle-size distributions of the (a) FeCoCrNi and (b) FeCoCrNiMo<sub>0.5</sub> HEA powders. (c) Laser powder bed fusion (LPBF) equipment. (d) Schematic of the process flow and interlayer rotation. (e) Dimensions of the LPBF bar used to measure the high-temperature tensile strength. Structural characterization of (f) FeCoCrNi and (g) FeCoCrNiMo<sub>0.5</sub>: (f1, g1) inverse pole figures, (f2, g2) microstructures, (f3, g3) selected area electron diffraction patterns, and (f4, g4) X-ray diffraction patterns of the printed samples.

and brittle phases, including the  $\sigma$  phase and carbides like Mo<sub>2</sub>C and Cr<sub>23</sub>C<sub>6</sub>. Further, Cai et al. [27] fabricated an FeCoCrNiMo<sub>0.23</sub> HEA using a powder metallurgical method and demonstrated its good ductility (elongation = 51%) and ultimate tensile strength (UTS = 784 MPa) owing to nano-twin and microband generation during its tensile deformation. Chen et al. [28] synthesized an FeCoCrNiMo<sub>0.5</sub> HEA by LPBF and demonstrated its improved strength (UTS = 1110 MPa) and good plasticity (elongation = 30.1%) owing to the formation of a few nanoparticle precipitates. Thus, FeCoCrNiMo HEAs synthesized by LPBF exhibit excellent room-temperature performance. However, there has been little research on the high-temperature mechanical performance of LPBF-FeCoCrNiMo HEAs.

In this study, we designed and fabricated an FeCoCrNiMo<sub>0.5</sub> HEA (Mo content of 11.12 at%) by LPBF and evaluated its high-temperature

mechanical properties. The study findings indicate that the FeCoCrNiMo<sub>0.5</sub> HEA has better high-temperature mechanical properties than the existing HEAs and other common high-temperature alloys. The effect of the alloy microstructure on the high-temperature performance and deformation mechanism of the FeCoCrNiMo<sub>0.5</sub> HEA were also investigated.

## 2. Materials and methods

FeCoCrNi and FeCoCrNiMo<sub>0.5</sub> HEA powders with spherical particles of a nominal size (15–53  $\mu\text{m}$ ) were synthesized via a gas-atomization process. The samples were formed on a RENISHAW AM-400 LPBF platform (Fig. 1(c)) using the following process parameters: substrate preheating temperature = 120 °C, laser power = 200 W, line spacing =

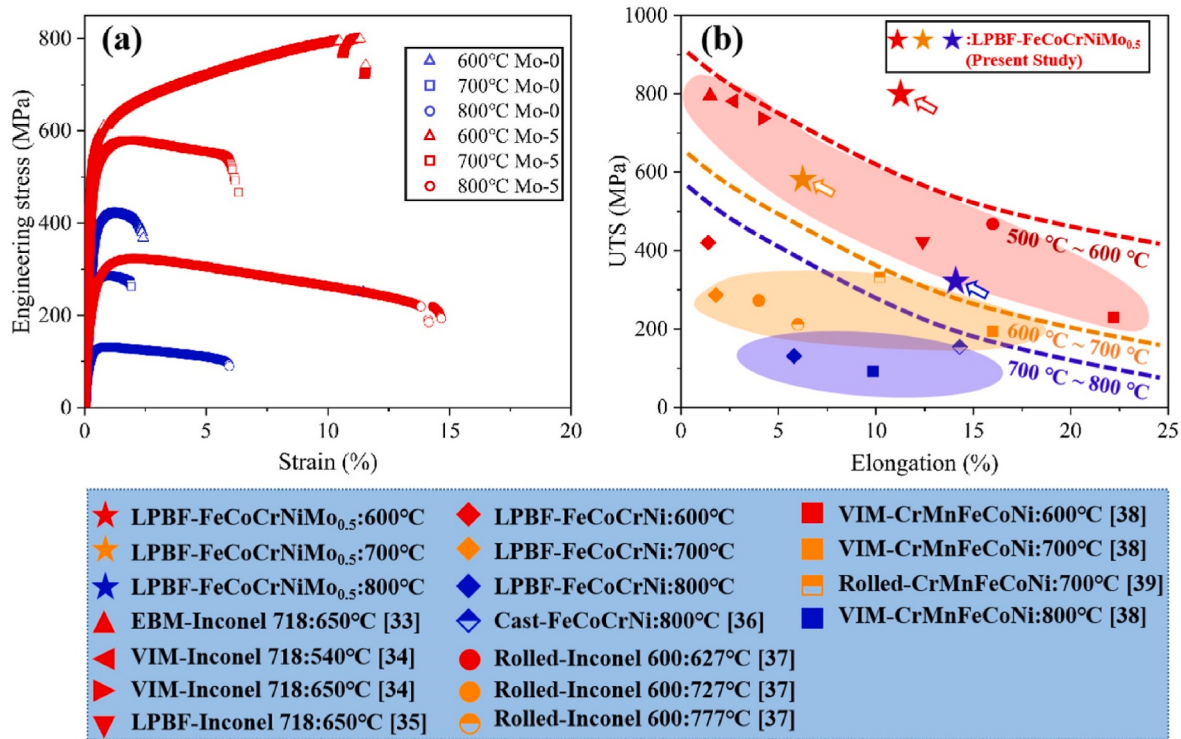


**Fig. 2.** (a) Comparison of the engineering stress–strain curves of FeCoCrNiMo<sub>0.5</sub> (Mo-5) and FeCoCrNi (Mo-0) recorded during high-temperature tensile testing (strain rate of  $8.33 \times 10^{-5} \text{ s}^{-1}$ ) at 600, 700, and 800 °C. (b) Comparison of the ultimate tensile strength (UTS) and elongation at elevated temperatures of the Mo-5 and some commonly used high-temperature alloys and high-entropy alloys (EBM: electron beam melting; VIM: vacuum induction melting).

80 μm, point spacing = 60 μm, exposure time = 80 μs, wavelength = 1070 nm, layer thickness = 40 μm, and interlayer rotation angle = 67° (Fig. 1(d)). Fig. 1(a) and (b) show the scanning electron microscopy (SEM) images of the two HEA powders produced using these parameters. Tensile testing was conducted on a 3910-type microcomputer-controlled electronic universal testing machine in the temperature range of 600–900 °C, and the high-temperature tensile strain rate was  $8.33 \times 10^{-5} \text{ s}^{-1}$ . SEM coupled with electron backscatter diffraction (EBSD) was conducted to characterize the morphologies of the pristine and mixed powders, as well as the as-printed samples and the samples subjected to tensile testing. Energy-dispersive X-ray spectrometry (EDS) was

performed to analyze the chemical compositions of the samples. Bright-field transmission electron microscopy (BF-TEM) was conducted to characterize the crystal structures and dislocation morphologies of the matrix phase and secondary phases.

### 3. Results and discussion

Fig. 1(f1) and (g1) show the inverse pole figures of the as-printed FeCoCrNi and FeCoCrNiMo<sub>0.5</sub> HEA samples (hereafter referred to as Mo-0 and Mo-5, respectively) along the X-Z plane. The microstructures of the two samples generally exhibit columnar grains and a tendency for

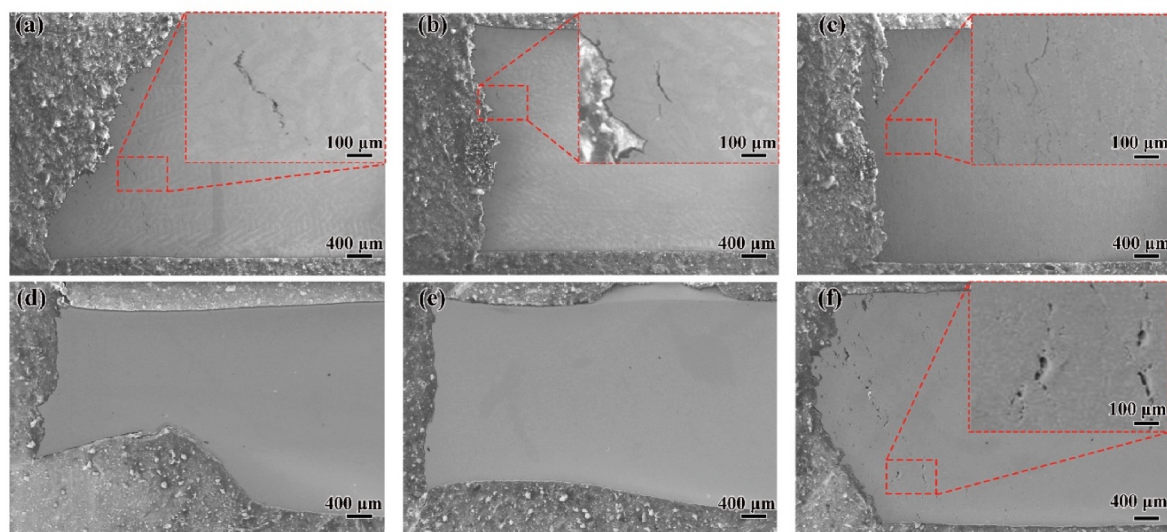


**Fig. 3.** Microstructures of the tensile fracture cross sections of the Mo-0 and Mo-5 samples subjected to tensile deformation at different temperatures: (a–c) Mo-0 after tensile testing at 600, 700, and 800 °C, respectively; (d–f) Mo-5 after tensile testing at 600, 700, and 800 °C, respectively.

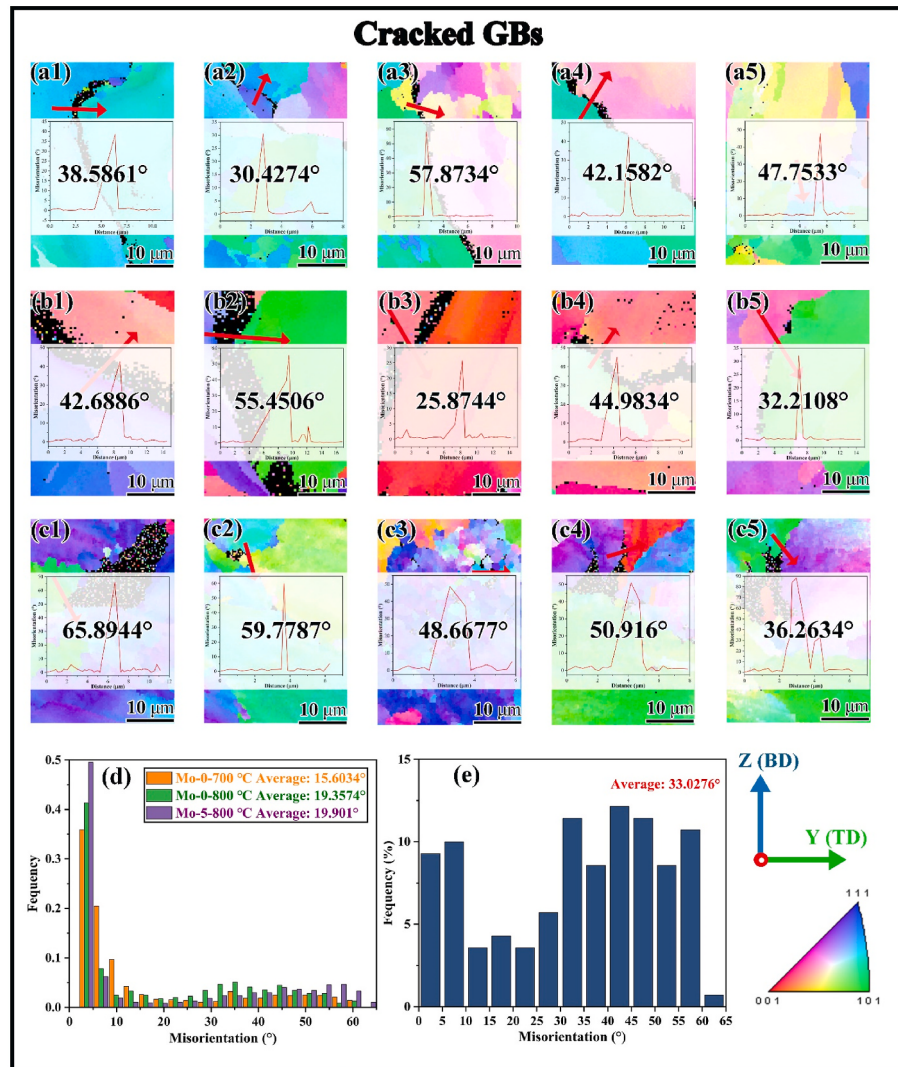


**Fig. 4.** Inverse pole figure maps and measured angles of cracked GBs (140 cracks were examined via EBSD, and 15 typical cracked GBs are shown based on their frequency of occurrence): (a1–a5) Mo-0 after tensile testing at 700 °C; (b1–b5) Mo-0 after tensile testing at 800 °C; and (c1–c5) Mo-5 after tensile testing at 800 °C. (d) Distribution of GB misorientation in LPBF specimens. (e) Distribution of cracked GB misorientation in LPBF specimens.

vertical growth, but the grains in Mo-5 are clearly refined. In the BF-TEM image of the Mo-0 MEA (Fig. 1(f2)), no precipitate phase is observed at the dislocation network position, and the SAED pattern in Fig. 1(f3) reveals that the microstructure of Mo-0 in the dislocation network position has a face-centered cubic (FCC) structure. In contrast, Mo-5 exhibits a net-like precipitate phase at the dislocation network positions, and the selected position corresponds to the  $\sigma$  phase (Fig. 1(g2, g3)). According to the SAED pattern of Mo-5, the hard intermetallic phase is the  $\sigma$  phase with a tetragonal structure, and the matrix retained its FCC structure.

Fig. 2(a) shows the tensile stress-strain curves of the printed Mo-0 and Mo-5 samples, recorded at the temperatures of 600, 700, and 800 °C. A significant difference is observed in the high-temperature tensile performances of Mo-5 and Mo-0. The strengths of both Mo-5 and Mo-0 decreased significantly with increasing temperature; however, their yield and tensile strengths at the same temperature differed significantly. Compared with the yield strength and UTS values of Mo-0, those of Mo-5 increased by 46.3 and 90.1%, respectively, at 600 °C, by 85.5 and 102.1%, respectively, at 700 °C, and by 52.9 and 146.6%, respectively, at 800 °C. The plasticities of Mo-0 and Mo-5 exhibited an increasing trend with increasing temperature, but a decrease in plasticity was observed at 700 °C for both samples. Specifically, both

samples showed a significant decrease in plasticity between 600 and 700 °C; however, the plasticity increased significantly at 800 °C (elongation = 14.1%), particularly for Mo-5. Fig. 2(b) compares the UTS and elongation of Mo-5 at elevated temperatures with those of commonly used high-temperature alloys and HEAs [34–40]. The Mo-5 sample synthesized by the LPBF process in this study has excellent overall performance in all temperature ranges, and it exhibits higher strength and greater ductility than the other samples.

To further explore the deformation mechanism of Mo-5 at high temperatures, the microstructures of Mo-0 and Mo-5 were compared after they were subjected to high-temperature tensile testing at the strain rate of  $8.33 \times 10^{-5} \text{ s}^{-1}$ . Fig. 3 shows the fracture surface morphologies of Mo-0 and Mo-5 after tensile testing at different temperatures. Cracks and pores were evident on the fracture surface of Mo-5 subjected to tensile testing at 800 °C (Fig. 3(f)), but not on those subjected to tensile deformation at 600 °C and 700 °C. In contrast, the fracture surface of Mo-0 exhibited distinct cracks and pores after high-temperature tensile testing at 600 °C (Fig. 3(a–c)), clearly indicating that the addition of Mo can effectively improve the GB strength and reduce the susceptibility of the FeCoCrNi HEA to crack. Mazánová et al. [41] reported that cracks are more likely to develop at high-angle grain boundaries (GBs). A comparison of the GB angles at the cracks in Mo-0

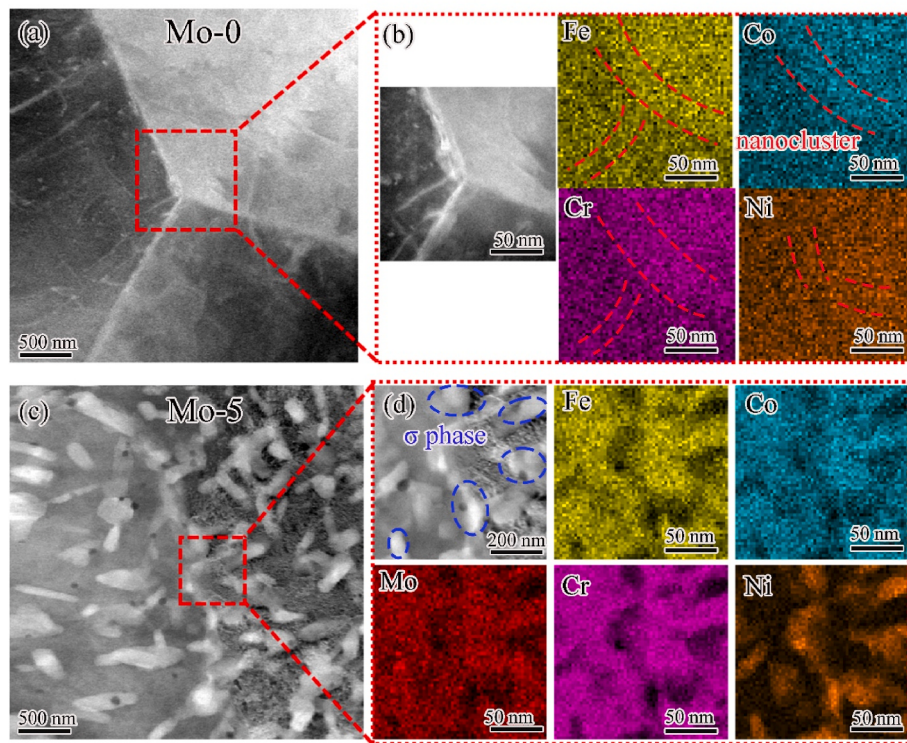


**Fig. 5.** Deformed microstructures and composition distribution, respectively, of (a and b) Mo-0 and (c and d) Mo-5 subjected to tensile testing at 800 °C.

and Mo-5 (Fig. 4(a1–c5)) subjected to tensile testing at different high temperatures confirmed that cracks occurred at high-angle GBs. To investigate the relationship between the GB angles and crack formation, 140 cracks in the LPBF specimens were statistically analyzed by EBSD. Fig. 4(d) shows the overall GB angle distribution of Mo-0 and Mo-5 after tensile testing at different temperatures. The low-angle GBs accounted for a large fraction of cracks owing to the occurrence of numerous dislocations in the microstructure during tensile deformation. However, statistics related to the GB angle at the crack initiation location (Fig. 4(e)) indicated that the high-angle GBs accounted for 80.7% of the total number of cracks, with the average GB being 33.0276°. This result suggests that the tensile fracture characteristics of the Mo-0 and Mo-5 HEAs correlate with their GB angles.

Ming et al. [42] reported that GB nanoclusters represent the main cause of high-temperature plasticity loss in FCC-structured HEAs. This is because of the enrichment of the elements at the GBs during the high-temperature tensile process, resulting in a weakened GB interface and micropore formation. Dense micropore defects are then connected to form crack sources. A similar phenomenon was observed in the cases of Mo-0 and Mo-5, in which cracks were generated at the GBs. Fig. 5(a) shows that Fe, Co, Cr, and Ni formed distinct nanoclusters at the GBs of Mo-0. Further, Fig. 5(b) shows the BF-TEM microstructure and EDS data of the GB of Mo-5 after high-temperature tensile deformation at 800 °C. Notably, it is impossible to accurately determine whether the elements at the GB retain their nanocluster structures after Mo addition because of the formation of the σ phase at the GB. A comparison of the high-temperature plasticities of Mo-0 and Mo-5 at different temperatures revealed that, overall, the high-temperature plasticity of Mo-5 increased with increasing Mo content. Determining whether the nanoclusters remained at the GBs is difficult. However, with the addition of Mo, the σ phase was diffusely cross-distributed at the GBs, as shown in Fig. 5(c). The distribution of the σ phase strengthened the GBs and prevented crack extension during deformation. The effects of the σ phase and twin deformation mechanism (described later) effectively mitigated the plasticity degradation caused by nanoclusters at 700 °C.

According to the uniform tensile deformation microstructure

presented in Fig. 6, the number of dislocation networks and entanglements in Mo-0 and Mo-5 decreased during high-temperature tensile testing, and a twinning structure was formed in Mo-5. As a slip source, twins guide dislocation slip, effectively reducing lattice distortion in grains and promoting the plastic deformation of the material. This also contributed significantly to the improved plasticity of Mo-5. When the test temperature reached 700 °C, the substructure became sparse, a portion of the secondary phase was transformed into a granular one, and the number of twins was increased (Fig. 6(d)). However, twins cannot pass through the σ phase during movement, and the tetragonal σ phase cannot synergistically deform with the FCC-structured matrix. These inabilities result in stress concentration at the grain interfaces. By contrast, at 800 °C (Fig. 6(e)), the resistance to atomic migration decreased, leading to reduced resistance between the σ phase and matrix, which facilitated the deformation of the HEA. In addition, the complete transformation of the σ phase from a strip-like form to a granular one and the reduced number of twins led to minimized dislocation hindrance and local stress concentration, which increased the high-temperature plasticity of the HEA. At the same time, due to the accumulation of deformation energy at 800 °C, dynamic recrystallization occurred in the system, which further improved the plasticity of the alloy at this temperature.

For Mo-5, i.e., the FeCoCrNiMo<sub>0.5</sub> HEA, the strip-shaped σ phase was observed at 600 °C (Fig. 6(c)), and numerous dislocations were found to accumulate at the interface between the σ phase and matrix, indicating that the strip-shaped σ phase significantly hindered the movement of dislocations. Further observations revealed that the dislocations did not pass through the σ phase, suggesting that the σ phase is responsible for Orowan strengthening. Moreover, lamellar structures, identified as twins, were observed in the deformed microstructure of Mo-5. According to previous studies [43–45], the deformation mechanisms of FCC-structured alloys are closely related to their stacking fault energy (SFE). The SFE determines how difficult it is for stacking faults and twins to form. With increasing SFE, the deformation mechanism transforms from dislocation slip ( $SFE \geq 40 \text{ mJ/m}^2$ ) to dislocation slip combined with deformation twin ( $20 \text{ mJ/m}^2 \leq SFE \leq 40 \text{ mJ/m}^2$ ) and dislocation

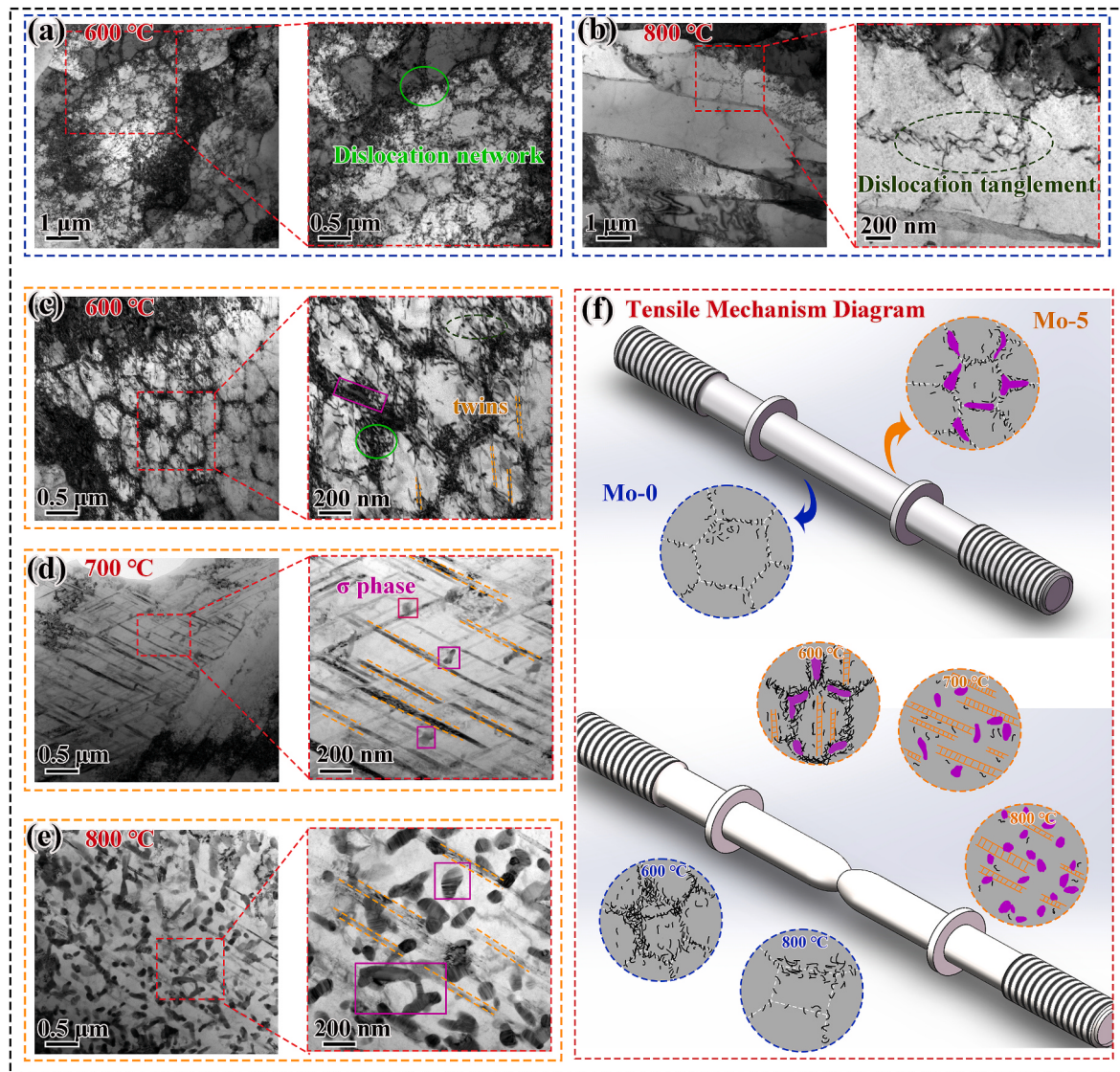


**Fig. 6.** High-temperature tensile deformation microstructures and deformation mechanisms of the FeCoCrNi (Mo-0) and FeCoCrNiMo0.5 (Mo-5) HEAs: (a, b) Mo-0 after tensile testing at 600 °C and 800 °C, respectively; (c, d, e) Mo-5 after tensile testing at 600, 700, and 800 °C, respectively. (f) Deformation mechanism of the HEA.

slip combined with phase transformation ( $SFE \leq 20 \text{ mJ/m}^2$ ) [45]. Zadach [43] calculated the SFE of an FeCoCrNiMn HEA by combining experimental and theoretical data, while Gao et al. [45] calculated the SFE of an FeCoCrNiMox HEA using X-ray diffraction (XRD) data. In this study, we similarly calculated the SFE values of Mo-0 and Mo-5 using Eqs. (1) and (2).

$$\gamma = \frac{K_{111_{\alpha_0}} G_{(111)} \alpha_0 A^{-0.37}}{\pi \sqrt{3}} \bullet \frac{\varepsilon^2}{\alpha} \quad (1)$$

$$\Delta 2\theta = \Delta(2\theta_{200} - 2\theta_{111}) = -\frac{45\sqrt{3}}{\pi^2} \left( \tan \theta_{200} + \frac{1}{2} \tan \theta_{111} \right) \alpha \quad (2)$$

where  $K_{111_{\alpha_0}}$  is the proportional constant ( $=6.6$ ), and  $G_{(111)}$  is the shear modulus of the (111) plane (the macro-shear moduli of Mo-0 and Mo-5 were calculated as 84.87 and 90.34 GPa, respectively, using JMatPro software). Further,  $\alpha_0$  is the lattice constant determined by XRD (Fig. 2 (c-f)),  $A$  is a constant ( $=3.43$ ) related to anisotropy,  $\varepsilon$  is the microstrain determined from the Williamson–Hall plot obtained based on the XRD profiles,  $\alpha$  is the probability of stacking faults being formed, and  $\theta_{hkl}$  is the hkl plane of the FCC phase, as determined by XRD.

The SFE values of Mo-0 and Mo-5 were calculated to be 32.5 and 17.9, respectively. At the same time, the comparison of the microstructures revealed that as the deformation temperature was increased continuously, the dislocation network essentially disappeared at 700 °C, and no dislocation structure was observed at 800 °C. Further, the number of twins increased significantly, confirming that the deformation mechanism of the FeCoCrNi HEA was changed from dislocation-motion-dominant to twinning-dominant deformation after the addition of Mo. Literature survey on similar changes in the deformation mechanisms of alloys revealed that the size and number of twins observed in the HEAs examined in this study were similar to those observed in other studies [46–48]. Thus, the LPBF-FeCoCrNiMo<sub>0.5</sub> HEA exhibited improved strength and plasticity. In addition, owing to the characteristics of rapid solidification under the LPBF process, the σ phase served as the crystal nuclei, increasing the nucleation rate of the HEA grains. Furthermore, crystal growth was limited because of the rapid solidification speed of the alloy, and thus abundant nuclei were formed. This contributed to the aforementioned grain refinement of Mo-5. The solid-solution strengthening effect derived from Mo, the Orowan strengthening effect and grain refinement derived from the precipitation of the σ phase, and the twinning-induced strengthening effect derived

from the reduction in the SFE are the main reasons for the improved strength of Mo-5.

Fig. 6(f) illustrates the high-temperature deformation mechanisms of the Mo-0 and Mo-5 HEAs. As the HEA was heated, the alloy microstructure changed significantly at 800 °C, the dislocation network structure disappeared, and the density of the σ phase increased substantially. The strip-shaped σ phase nearly disappeared, and numerous granular σ phases precipitated. Further, the number of twins decreased, and the twins appeared to have passed through the σ phase. However, because the σ phase and twins have different crystal structures, twins cannot pass through the σ phase. Thus, we infer that the granular σ phase was formed after twin formation. The inhibitory effect of the granular σ phase on dislocation was clearly reduced, which in turn decreased the high-temperature strength of the HEA. In summary, the morphological transformation of the σ phase from a strip-like form to a granular one, decreased dislocation entanglement, and the reduced number of twins led to decreased high-temperature strength of Mo-5. However, Mo-5 still had a significantly greater high-temperature strength than Mo-0 because of the presence of secondary phases and twinning microstructures in its matrix.

#### 4. Conclusions

In this study, FeCoCrNi and FeCoCrNiMo<sub>0.5</sub> HEAs were synthesized by LPBF, and their high-temperature mechanical performances were evaluated. The strengthening mechanisms of the two HEAs (with and without Mo) were also investigated. The LPBF-FeCoCrNiMo<sub>0.5</sub> HEA was found to have a lower SFE than the LPBF-FeCoCrNi HEA, and twins were observed in the deformed microstructure of the former. Cracking usually occurred at high-angle GBs, and the dominant deformation mechanism changed from dislocation motion to twinning after the addition of Mo to FeCoCrNi. The precipitation of the σ phase resulted in high strength and ductility of the LPBF-FeCoCrNiMo<sub>0.5</sub> HEA at elevated temperatures. In particular, at 800 °C, the FeCoCrNiMo<sub>0.5</sub> HEA exhibited a 146.6% increase in high-temperature strength and 137.6% increase in elongation compared with those of the LPBF-FeCoCrNi HEA sample without Mo.

#### CRediT authorship contribution statement

**Danyang Lin:** Writing – review & editing, Methodology, Funding acquisition, Conceptualization. **Qi Chen:** Writing – review & editing, Writing – original draft. **Xin Xi:** Writing – review & editing, Writing – original draft. **Rui Ma:** Resources, Project administration. **Zhifeng Shi:** Writing – review & editing. **Xiaoguo Song:** Writing – review & editing. **Hongbo Xia:** Project administration. **Hong Bian:** Writing – review & editing. **Caiwang Tan:** Project administration. **Yongxin Lu:** Writing – review & editing. **Runsheng Li:** Writing – review & editing.

#### Declaration of competing interest

The authors declare that they have no known competing financial interests or personal relationships that could have appeared to influence the work reported in this paper.

#### Data availability

No data was used for the research described in the article.

#### Acknowledgments

This study was supported by the National Natural Science Foundation of China (Grant No. 52205348) and Natural Science Foundation of Shandong Province (Nos. ZR2023JQ021 and ZR2022QE087).

#### References

- [1] Y. Xiong, K. Shu, Y. Li, Z. Chen, X. Zha, T. He, S. Han, C. Wang, Deformation temperature impacts on the microstructure evolution and mechanical properties of a novel medium-heavy alloy (MHA), Mater. Sci. Eng., A 856 (2022) 144005.
- [2] Z. Li, Q. Kang, Y. Chen, X. Xv, T. Zhou, G. Wang, The microstructure evolution and the effect of grain size, temperature, and TiB<sub>2</sub> on the deformation mechanism of TiB<sub>2</sub>/TA15 composites during high temperature deformation, Mater. Sci. Eng., A 878 (2023) 145213.
- [3] L. Li, H. Chen, Q. Fang, J. Li, F. Liu, Y. Liu, P.K. Liaw, Effects of temperature and strain rate on plastic deformation mechanisms of nanocrystalline high-entropy alloys, Intermetallics 120 (2020) 106741.
- [4] R. John, M.K. Dash, B.S. Murty, D. Fabijanic, Effect of temperature and strain rate on the deformation behaviour and microstructure of Al0.7CoCrFeNi high entropy alloy, Mater. Sci. Eng., A 856 (2022) 143933.
- [5] J.W. Yeh, S.K. Chen, S.J. Lin, J.Y. Gan, T.S. Chin, T.T. Shun, C.H. Tsau, S.Y. Chang, Nanostructured high-entropy alloys with multiple principal elements: novel alloy design concepts and outcomes, Adv. Eng. Mater. 6 (2004) 299–303.
- [6] D.B. Miracle, O.N. Senkov, A critical review of high entropy alloys and related concepts, Acta Mater. 122 (2017) 448–511.
- [7] J. Liu, Z. Li, D. Lin, Z. Tang, X. Song, P. He, S. Zhang, H. Bian, W. Fu, Y. Song, Eutectic high-entropy alloys and their applications in materials processing engineering: a review, J. Mater. Sci. Technol. 189 (2024) 211–246.
- [8] L. Zhang, Y. Xiang, J. Han, D.J. Srolovitz, The effect of randomness on the strength of high-entropy alloys, Acta Mater. 166 (2019) 424–434.
- [9] M. Vaidya, K.G. Pradeep, B.S. Murty, G. Wilde, S.V. Divinski, Bulk tracer diffusion in CoCrFeNi and CoCrFeMnNi high entropy alloys, Acta Mater. 146 (2018) 211–224.
- [10] G. Laplanche, S. Berglund, C. Reinhart, A. Kostka, F. Fox, E.P. George, Phase stability and kinetics of a sigma-phase precipitation in CrMnFeCoNi high-entropy alloys, Acta Mater. 161 (2018) 338–351.
- [11] Y. Kim, Y. Joo, H.S. Kim, K. Lee, High temperature oxidation behavior of Cr-Mn-Fe-Co-Ni high entropy alloy, Intermetallics 98 (2018) 45–53.
- [12] Y. Kao, S. Chen, J. Sheu, J. Lin, W. Lin, J. Yeh, S. Lin, T. Liou, C. Wang, Hydrogen storage properties of multi-principal-component CoFeMnTiV<sub>y</sub>Zr<sub>x</sub> alloys, Int J Hydrogen Energ 35 (2010) 9046–9059.
- [13] L. Guo, X. Ou, S. Ni, Y. Liu, M. Song, Effects of carbon on the microstructures and mechanical properties of FeCoCrNiMn high entropy alloys, Mat Sci Eng A-Struct 746 (2019) 356–362.
- [14] T. DebRoy, H.L. Wei, J.S. Zuback, T. Mukherjee, J.W. Elmer, J.O. Milewski, A. M. Beese, A. Wilson-Heid, A. De, W. Zhang, Additive manufacturing of metallic components - process, structure and properties, Prog. Mater. Sci. 92 (2018) 112–224.
- [15] X. Xi, D. Lin, X. Song, X. Luo, R. Ma, Z. Shi, H. Bian, W. Fu, Z. Dong, C. Tan, Strength-plasticity transition mechanism after the solution treatment of GH3230 superalloy fabricated via laser powder bed fusion, Mater. Sci. Eng., A 876 (2023) 145124.
- [16] Danyang Lin, X. Xi, M. Yan, R. Ma, Z. Shi, Z. Tang, Z. Li, C. Tan, Z. Dong, X. Song, Significantly improved weldability in laser welding of additively manufactured haynes 230 superalloys by tailoring microstructure, J. Mater. Res. Technol. 26 (2023) 7873–7892.
- [17] Y. Brif, M. Thomas, I. Todd, The use of high-entropy alloys in additive manufacturing, Scripta Mater. 99 (2015) 93–96.
- [18] P.F. Xie, M.P. Yin, Y. Zhao, Y. Liu, Y. Qi, X.N. Li, C.X. Li, G. Wu, Removal of covered metallic stents with a bullet head for bronchopleural fistula using a fluoroscopy-assisted interventional technique, Clin. Radiol. 75 (2020).
- [19] M. Tekin, G. Polat, Y.E. Kalay, H. Kotan, Grain size stabilization of oxide dispersion strengthened CoCrFeNi-Y(2)O<sub>3</sub> high entropy alloys synthesized by mechanical alloying, J Alloy Compd 887 (2021).
- [20] J. He, Y. Qiao, R. Wang, Y. Tang, S. Li, X. Liu, Y. Ye, L. Zhu, Z. Wang, S. Bai, State and effect of oxygen on high entropy alloys prepared by powder metallurgy, J Alloy Compd 891 (2022).
- [21] D. Lin, X. Xi, X. Li, J. Hu, L. Xu, Y. Han, Y. Zhang, L. Zhao, High-temperature mechanical properties of FeCoCrNi high-entropy alloys fabricated via selective laser melting, Mater. Sci. Eng., A 832 (2022) 142354.
- [22] X. Zhu, G. Wang, X. Wang, G. Zhao, Microstructure and mechanical properties of Al<sub>0.3</sub>FeCoCrNi high entropy alloy processed by laser powder bed fusion using FeCoCrNi and Al powder mixture, Mater. Sci. Eng., A 848 (2022) 143468.
- [23] J. Man, B. Wu, G. Duan, L. Zhang, G. Wan, L. Zhang, N. Zou, Y. Liu, The synergistic addition of Al, Ti, Mo and W to strengthen the equimolar CoCrFeNi high-entropy alloy via thermal-mechanical processing, J Alloy Compd 902 (2022) 163774.
- [24] D. Lin, L. Xu, X. Li, H. Jing, G. Qin, H. Pang, F. Minami, A Si-containing FeCoCrNi high-entropy alloy with high strength and ductility synthesized in situ via selective laser melting, Addit. Manuf. 35 (2020) 101340.
- [25] C. Ren, K. Sun, Y.F. Jia, N.Z. Zhang, Y.D. Jia, G. Wang, Effect of Mo addition on the microstructural evolution and mechanical properties of Fe-Ni-Cr-Mn-Al-Ti high entropy alloys, Mater. Sci. Eng., A 864 (2023) 144579.
- [26] Y.B. Peng, W. Zhang, X.L. Mei, H.J. Wang, M.Y. Zhang, L. Wang, X.F. Li, Y. Hu, Microstructures and mechanical properties of FeCoCrNi-Mo High entropy alloys prepared by spark plasma sintering and vacuum hot-pressed sintering, Mater. Today Commun. 24 (2020) 101009.
- [27] B. Cai, B. Liu, S. Kabra, Y. Wang, K. Yan, P.D. Lee, Y. Liu, Deformation mechanisms of Mo alloyed FeCoCrNi high entropy alloy: in situ neutron diffraction, Acta Mater. 127 (2017) 471–480.
- [28] X. Chen, Y. Liang, Q. Wang, K. Dong, Y. Yang, S. Feng, X. Zhang, Y. Cai, Y. Peng, K. Wang, J. Kong, Introduction of nanoprecipitation into supersaturated

- CoCrFeNiMo0.5 alloy prepared by laser-powder bed fusion via microstructure tailoring to achieve excellent properties, *Scripta Mater.* 235 (2023) 115636.
- [29] D. Lin, X. Xi, R. Ma, Z. Shi, H. Wei, X. Song, S. Hu, C. Tan, Fabrication of a strong and ductile FeCoCrNiMo0.3 high-entropy alloy with a micro-nano precipitate framework via laser powder bed fusion, *Compos. B Eng.* 266 (2023) 111006.
- [30] A. Piglione, B. Dovgyy, C. Liu, C.M. Gourlay, P.A. Hooper, M.S. Pham, Printability and microstructure of the CoCrFeMnNi high-entropy alloy fabricated by laser powder bed fusion, *Mater. Lett.* 224 (2018) 22–25.
- [31] Y. Guan, X. Cui, D. Chen, W. Su, Y. Zhao, J. Li, G. Jin, Preparation of hypereutectic-eutectic-hypoeutectic gradient high-entropy alloy coating by in-situ interfacial reaction between Nb and FeCoCrNi, *Mater. Lett.* 346 (2023) 134573.
- [32] R. Fan, L. Wang, L. Zhao, L. Wang, S. Zhao, Y. Zhang, B. Cui, Synergistic effect of Nb and Mo alloying on the microstructure and mechanical properties of CoCrFeNi high entropy alloy, *Mater. Sci. Eng., A* 829 (2022) 142153.
- [33] M. Abdullah, M. Mukarram, T.B. Yaqub, F. Fernandes, K. Yaqoob, Development of eutectic high entropy alloy by addition of W to CoCrFeNi HEA, *Int. J. Refract. Metals Hard Mater.* 115 (2023) 106300.
- [34] S. Sun, Y. Koizumi, T. Saito, K. Yamanaka, Y. Li, Y. Cui, A. Chiba, Electron beam additive manufacturing of Inconel 718 alloy rods: impact of build direction on microstructure and high-temperature tensile properties, *Addit. Manuf.* 23 (2018) 457–470.
- [35] S. Lee, S. Chang, T. Tang, H. Ho, J. Chen, Improvement in the microstructure and tensile properties of inconel 718 superalloy by HIP treatment, *Mater. Trans.* 47 (2006) 2877–2881.
- [36] Q. Teng, S. Li, Q. Wei, Y. Shi, Investigation on the influence of heat treatment on Inconel 718 fabricated by selective laser melting: microstructure and high temperature tensile property, *J. Manuf. Process.* 61 (2021) 35–45.
- [37] X.W. Liu, N. Gao, J. Zheng, Y. Wu, Y.Y. Zhao, Q. Chen, W. Zhou, S.Z. Pu, W. M. Jiang, Z.T. Fan, Improving high-temperature mechanical properties of cast CrFeCoNi high-entropy alloy by highly thermostable in-situ precipitated carbides, *J. Mater. Sci. Technol.* 72 (2021) 29–38.
- [38] S.A. Chavez, D.M. Harper, G.E. Korth, High-temperature tensile and creep data for Inconel 600, 304 stainless steel and SA106B carbon steel, *Nucl. Eng. Des.* 148 (1994) 351–363.
- [39] J.H. Kim, K.R. Lim, J.W. Won, Y.S. Na, H. Kim, Mechanical properties and deformation twinning behavior of as-cast CoCrFeMnNi high-entropy alloy at low and high temperatures, *Mater. Sci. Eng., A* 712 (2018) 108–113.
- [40] M.J. Jang, S. Praveen, H.J. Sung, J.W. Bae, J. Moon, H.S. Kim, High-temperature tensile deformation behavior of hot rolled CrMnFeCoNi high-entropy alloy, *J Alloy Compd* 730 (2018) 242–248.
- [41] V. Mazáňová, M. Heczko, J. Polák, On the mechanism of fatigue crack initiation in high-angle grain boundaries, *Int J Fatigue* 158 (2022) 106721.
- [42] K. Ming, L. Li, Z. Li, X. Bi, J. Wang, Grain boundary decohesion by nanoclustering Ni and Cr separately in CrMnFeCoNi high-entropy alloys, *Sci. Adv.* 5 (2019).
- [43] A.J. Zaddach, C. Niu, C.C. Koch, D.L. Irving, Mechanical properties and stacking fault energies of NiFeCrCoMn high-entropy alloy, *JOM-US* 65 (2013) 1780–1789.
- [44] W.H. Liu, Z.P. Lu, J.Y. He, J.H. Luan, Z.J. Wang, B. Liu, Y. Liu, M.W. Chen, C.T. Liu, Ductile CoCrFeNiMox high entropy alloys strengthened by hard intermetallic phases, *Acta Mater.* 116 (2016) 332–342.
- [45] X. Gao, T. Liu, X. Zhang, H. Fang, G. Qin, R. Chen, Precipitation phase and twins strengthening behaviors of as-cast non-equiautomic CoCrFeNiMo high entropy alloys, *J Alloy Compd* 918 (2022) 165584.
- [46] X. Wang, Y. Ding, Y. Gao, Y. Ma, J. Chen, B. Gan, Effect of grain refinement and twin structure on the strength and ductility of Inconel 625 alloy, *Mater. Sci. Eng., A* 823 (2021) 141739.
- [47] A. Dhal, B. Prathyusha, R. Kumar, S.K. Panigrahi, Twin evolution and work-hardening phenomenon of a bulk ultrafine grained copper with high thermal stability and strength-ductility synergy, *Mater. Sci. Eng., A* 802 (2021) 140622.
- [48] M. Dao, L. Lu, Y.F. Shen, S. Suresh, Strength, strain-rate sensitivity and ductility of copper with nanoscale twins, *Acta Mater.* 54 (2006) 5421–5432.